Figure 11(a) illustrates the evolution of the mean mixture fraction in the transverse direction at different axial flow positions in Case 1, noting that the turbulent mixture becomes very important above $x/D$p= 7.5 i.e. at the time of an outbreak of Kelvin-Helmholtz instabilities, meaning that a large amount of tracer has flooded the jet center. Outer and inner layers meet each other leading to the creation of a single layer of a mixture similar to a single round jet.

Figure 11(b) shows the profile of the mean mixture fraction in the transverse direction in different axial sections for Case 2, the figure shows that the majority of the mixture remains limited to the central jet, while a very small amount of tracer is found in the annular jet, and the tracer's transverse diffusion never reaches the ambient fluid, in which case the mixture does not benefit from the turbulent intensity at the external jet.

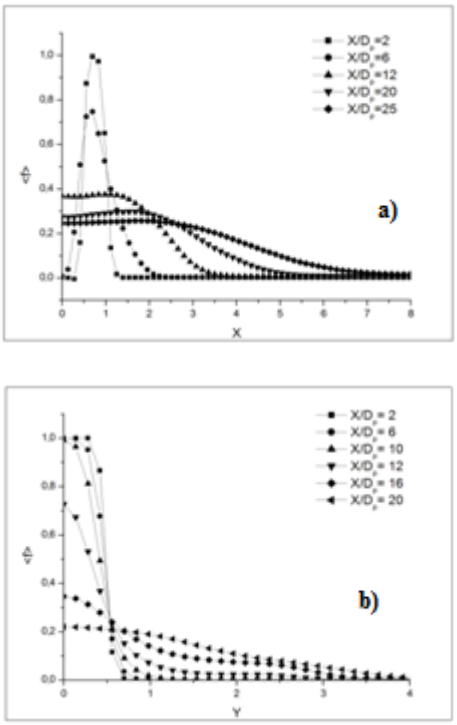


**Figure 11:** transverse evolution of mixture fraction for different $x/D$p positions: a) Case1, b) Case2

**4.5 RMS profiles of mixture fraction**

Figure 12: Longitudinal evolution of RMS of mixture fraction in annular jet (solid line) and central jet (discontinuous line): a) Case1, b) Case2

RMS longitudinal evolution of mixture fraction for the central and annular jet along with both the central and annular jet axis is shown in Figure 12(a) for Case 1, the growth of mixture fraction intensity for both jets increases to $x/D$p = 5 and the peak of maximum mixing intensity amplitude is reached when the internal and external shear layers fuse.

For Case2, Figure 12(b) shows the same scenario as Case 1.

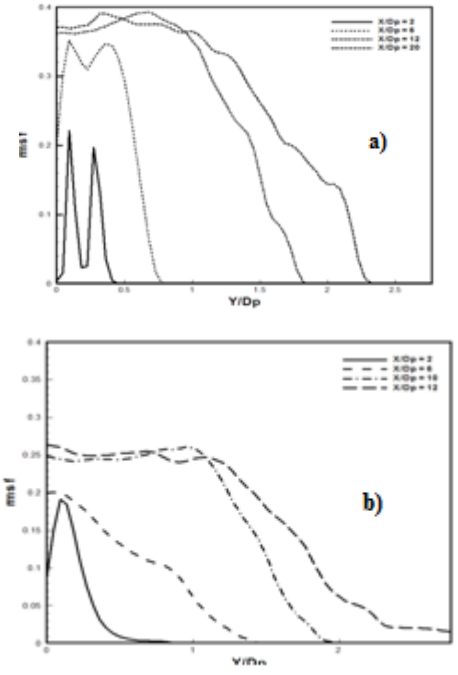


**Figure 12:** transverse evolution of mixture fraction for different $x/D$p positions: a) Case1, b) Case2

Mixture fraction RMS for different axial positions of Case 1 is illustrated in Figure 13(a). In addition, RMS profile at the beginning of the jet shows two distinct peaks located at the inner and outer sheared layers, respectively, the intensity of the two peaks is responsible for the turbulent mixing efficiency in the jet. Close to the nozzle inlet, and due to the blocking phenomenon. Figure 13(b) represents the mixture fraction RMS profile for different axial positions in Case 2. It can be seen that the mixture fraction fluctuation remains localised in the jet center and their intensity remains lower than when the tracer had been generated by the annular jet.

### 4.6 Mixing PDF probability function

PDFs were calculated at 5 different transverse positions extending from the center line of the primary jet to the edge of the jet structure.

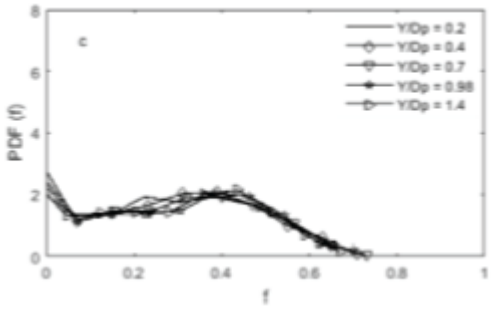


**Figure 13:** Mixture fraction PDF for (a) $x/D$p = 4 (b) $x/D$p = 7 and (c) $x/D$p = 20

Figure 14(a) shows PDF in the inner and outer sheared layers, In $x/D$p = 4. There is a very low probability of finding a value of different from the mean value because, in this region of the jet, there is no turbulent mixture yet.

Figure 14(b) shows PDF at the inner and outer shear layers at $x/D$p = 7. In different transverse positions, there is a wide range where the probability of finding a given value of the mixture fraction is non-zero. This is due to the turbulent mixing process associated with the formation of Kelvin-Helmholtz eddies in the two sheared layers. In this region, the mixture is not homogeneously distributed within large turbulence structures.

Figure 14(c) shows PDF at the level of the mixing layer created after the fusion of the two shear layers in $x/D$p = 20. In this region, PDF is characterised by most probable values of the mixture fraction almost independent of the transverse position through the sheared layers. This type of PDF was produced by the persistence of mixing at large turbulence structures. To the end of the calculation range where the fully developed state of turbulence is reached, it is observed that the mixture is not yet homogeneous.

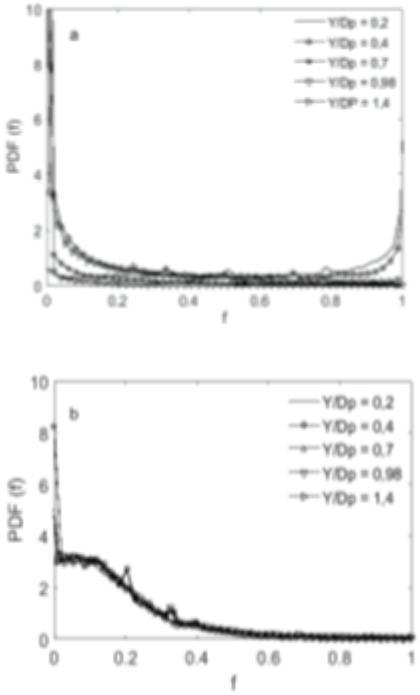


**Figure 14:** Fraction mixture PDF for (a) $x/D$p = 7 and (b) $x/D$p = 20

Case 2 PDF was also calculated when the tracer is injected in the central jet. Figure 15 (a) shows the mixed fraction PDF at the internal shear layer in $x/D$p = 7. Before, the fully developed state of turbulence. As a result, the probability of finding a given value of f is almost the same in the transverse direction. This shows that the tracer is not evenly distributed in the large eddies.

PDF in $x/D$p = 20. After the fusion of two shear layers and at the single shear layer and in different transverse positions, is shown in Figure 15 (b). There is a high probability of finding a given value of the mixture fraction. It is important to note that the probability of finding f=1 is zero in this flow region, meaning that the tracer is totally mixed in this region.

### 5. CONCLUSIONS

This study examined the mixing process in a compressible turbulent coaxial jet, where two cases were considered: a passive scalar injected at the annular jet Case 1 and a passive scalar injected at the central jet Case 2, using Smagorinsky numerical Large-Eddy Simulations (LES).

This study was articulated on investigated the implementation of a high-performance and modern numerical method, called the linearization solver of Riemann problem characteristic equations, which meets the requirements in terms of accuracy of results and calculation cost. White noise was overlaid at the laminar flow inlet to trigger jet disruption and the development of Kelvin-Helmholtz eddies.

As a result, the mixing process was analysed using the spatial and temporal resolution of the transport equation of the mixture fraction.

Therefore, Kelvin – Helmholtz eddies play a very important role in the mixing process. When the passive scalar is injected into the annular jet, the disturbances are small in the potential cone region and the mixture is mainly due to molecular diffusion. After the potential cone area, the natural development of instabilities is at the level of the internal and external shear layers and turbulent mixture is initiated by the emergence of Kelvin-Helmholtz eddies.

However, the mixture is not yet homogeneous in the fully developed turbulence region, which results in an ineffective mixture. Once the passive scalar is injected into the central jet, the mixing process is the same as in Case 1., but after the potential cone region only the vortices of the inner shear layer participate in the mixture and the vortices of the outer shear layer are surrounded only by the fluid from the surrounding air.

In this configuration the mixture is homogeneous in the fully developed turbulence region and the efficiency of the mixture is maintained. Results also showed that the active mixing regions are located between internal and external jets, external jet and ambient fluid. These regions were associated with high concentration root mean square (RMS) values.

The Riemann solver used in the present work was found to perform extremely well and is computationally inexpensive, making it suitable for practical applications where high accuracy and fast computation are needed.

The mixture is not yet homogeneous in the fully developed turbulence region if the tracer is injected into an annular jet. But it is homogeneous if the tracer is injected in the central jet.

A further step in this work would be the simulation of reactive flows. As a result, this work will be carried out by examining the implementation of different models of chemical kinetics and the lighting of the flame.

**REFERENCES**

[1] Warda, H.A., Kassab, S.Z., Elshorbagy, K.A., Elsaadawy, E.A. 1999. An experimental investigation of the near-field region of a free Turbulent coaxial jet using LDA. Flow Measurement and Instrumentation, 10, 15–26.

[2] Forstall, W., Shapiro, A.H. 1951. Momentum and mass transfer in coaxial gas jets. Journal of Applied Mechanics, 18, 219–239.

[3] Crow, C.S., Champagne, F.H. 1971. Orderly structure in jet turbulence. Journal of Fluid Mechanics, 48, 547–591.

[4] Villermaux, E., Rahab, H. 2000. Mixing in coaxial jets. Journal of Fluid Mechanics, 425, 161–185.

[5] Rehab, H., Villermaux, E., Hopfinger, E.J. 1997. Flow regimes and mixing in the near field of large velocity ratio coaxial jets. 11th Symposium on Turbulent Shear Flows, Grenoble, France, 8-10, septembre, 3(25), 7–10.

[6] Da Silva, C.B., Balarac, G., Metais, O. 2003. Transition in high velocity ration coaxial jets analysed from direct numerical simulations. Journal Turbulence, 4, 1–18.

[7] Balarac, G., Si-Ameur, M., Lesieur, M., Metais, O. 2007. Direct numerical simulations of high velocity ratio coaxial jets mixing properties and influence of upstream conditions. Journal of Turbulence, 8, 1–14.

[8] Dianat, M., Yang, Z., Jiang, D., Mcguirk, J.J. 2006. Large eddy simulation of scalar mixing in a coaxial confined jet Flow. Turblence Combustion, 77, 205–27.

[9] Jahnke, S., Kornev, N., Tkatchenko, I., Hassel, E., Leder, A. 2005. Numerical study of influence of different parameter on mixing in coaxial jet mixer using LES. Heat Mass Transfer, 41:471–481.

[10] Dinesh, K.K.J.R., Savill, A.M., Jenkins, K.W., Kirkpatrick, M.P. 2010. A study of mixing and intermittency in a coaxial turbulent jet. Fluid Dynamics Research, 42 (2).

[11] Segalini, A. 2010. Experimental analysis of coaxial jets: instability, flow and mixing characterization, PHD thesis, Uniiverrsiittà dii Bollogna.

[12] Shahbazian, N. 2015. Subfilter Scale Combustion Modelling for Large Eddy Simulation of Turbulent Premixed Flames, PHD thesis, Department of Aerospace Science and Engineering University of Toronto.

[13] Pietroniro, A.G. 2016. Modelling coaxial jets relevant to turbofan jet engines, Master of Science Thesis, Department of Mechanics Fluid Mechanics Stockholm.

[14] Milanovic, G. 2017. The Developing Region of a Turbulent Coaxial Jet, PHD thesis, McGill University, Montreal, Canada.

[15] Smagorinsky, J. 1963. General circulation experiments with the primitive equations. Monthly Weather Review, 91, 99–164.

[16] Kopchenov, V.I., Kraiko, A.N. 1983. A second-order monotone difference scheme for hyperbolic systems with two independent variables. USSR Computational Mathematics and Mathematical Physics, 23 (4), 50–56.

[17] Yanamoto, S., Daiguji, H. 1993. Higher order accurate upwind schemes for solving compressible Euler and Navier–Stokes equations. Computers & Fluids, 22(2/3), 259–270.

[18] Godunov, S.K. 1959. A difference scheme for numerical computation of discontinuous solution of hyperbolic equations. Matematicheskii Sbornik, 47, 271–306.

[19] Laney, C.B. 1993. Computational Gas Dynamics. Cambridge University Press.

[20] Mathur, S.R., Murthy, J.Y. 1997. A pressure-based method for unstructured meshes. Numerical Heat Transfer, 31, pp. 191–215.

[21] Lomax, H., Pulliam, T.H., Zingg, D.W. 2001. Fundamentals of Computational Fluid Dynamics. Springer-Verlag Berlin Heidelberg.

[22] Wesseling, P. 2001. Principles of Computational Fluid Dynamics. Verlag Berlin Heidelberg: Springer.

[23] Gropp, W., Lusk, E., Skjellum, A. 1999. Using MPI. Cambridge, Massachusetts: MIT Press.

[24] Nobes, M.I.J., Nathan, G.J. 2001. Influence of jet exit conditions on the passive scalar field of an axisymmetric free jet. Journal of Fluid Mechanics, 432, 91-125.

[25] Perez-Alvarado, A. 2016. Effect of background turbulence on the scalar field of a turbulent jet, PhD thesis, McGill University.

**NOMENCLATURE**

| | |
|---|---|
| $\theta_p$ | Momentum thickness of the primary jet |
| $\theta_s$ | Momentum thickness of the secondary jet |
| $B$ | The Limiter flux |
| $CFL$ | The Courant-Friedrichs-Lewy |

| | | | |
|---|---|---|---|
| e | The interne energy | $U_\infty$ | The velocity of air ambient |
| $F$ | The flux in x - direction | $U[\rho,\rho u,\rho v,\rho w,\rho e]$ | The filtered conserved vector |
| $G$ | The flux in y- direction | $w[\rho,u,v,w,p]$ | The primitives' variables |
| $H$ | The flux in z- direction | $\Delta x,\Delta y,\Delta z$ | Grid size |
| $M$ | Mach number | $x_i$ | The coordinate Cartesian x,y,z |
| $n$ | Number of time step | $t$ | The time t |
| $P$ | Pressure | Δt | The time iteration method |
| $Pr$ | Prandt number | VNN | The von Neumann number |
| $Pr_{sgs}$ | Prandt number of subgrid scale | $\nu_{sgs}$ | The turbulent eddy viscosity |
| $R_p$ | Inner radius of the coaxial jet | $\nu$ | Kinematic Viscosity molecular |
| $R_s$ | Outer radius of the coaxial jet | $\mu$ | Dynamical viscosity coefficient |
| $R_m$ | Average radius of the coaxial jet | $\tau_{ij}$ | SGS stress tensor |
| $Re$ | The Reynolds number | $\rho$ | Density |
| $S_{ij}$ | The strain rate tensor | $\gamma$ | Specific heat ratio |
| $T$ | Temperature | $\delta_{ij}$ | The Kronecker symbol |
| $T_p$ | Temperature of jet primary | Δ | The filter width of the LES filter |
| $T_\infty$ | Temperature of ambient air | $minimod$ | The minimod function |
| $u_i$i | The three velocity components | $\left(i \mp \frac{1}{2}\right)$ | The interface volume control |
| $U_s$ | The velocity of the primary jet | $(i,j)$ | Index of the three components |
| $U_P$ | The velocity of the secondary jet | $(\ )_{invis}$ | Index of In-viscid flux |